

Photometry and Supernovae: A case study

Naman Pratap, Gourav Kumawat, Rohan Sanghai, Sanatan,
Arnab Chowhan, Kushagra Sachan, Amit Deokar, Adbhut Vipin
Bhardwaj, Gaurav Badre, Aswin Suresh, Himadri Saha, Kunal
Deshmukh, Simran Joharle and Karthik J

Photometry and Supernovae: A case study

Copyright © 2020 Krittika IITB

PUBLISHED BY KRITTIKA: THE ASTRONOMY CLUB OF IIT BOMBAY

[GITHUB.COM/KRITTIKA IITB](https://github.com/KrittikaIITB)

First Release, November 2021



Contents

1	Introduction to CCDs and Image Reduction	5
1.1	CCD	5
1.2	Working	5
1.2.1	CCD Readout	6
1.2.2	Advantages of CCDs	7
1.3	Some Useful Terms	7
1.3.1	Quantum Efficiency	7
1.3.2	CCD Coatings	8
1.3.3	Gain and Linearity	8
1.3.4	Charge Diffusion and Charge Transfer Efficiency	8
1.3.5	Readout Noise and Dark Current	8
1.3.6	Bias	8
1.3.7	Full Well Capacity, Pixel Binning, Windowing	9
1.4	Signal-to-Noise Ratio	10
1.5	Image Data Reduction	10
1.6	References	11
2	PSF Photometry	13
2.1	What is PSF?	13
2.2	Why do we get the spread?	13
2.3	Significance of PSF	14
2.4	Performing PSF photometry	15

2.5	How is it beneficial?	16
3	Supernova theory	17
3.1	Search and Discovery of Supernovae	17
3.2	Classification of Supernovae	18
3.3	Photometry	18
3.4	Sites, Environments and Rates	18
3.5	Spectra	19
3.5.1	Elements of line formation in the Photospheric phase	19
3.5.2	Synthetic Spectra for the Photospheric Phase.	21
3.5.3	Detailed Calculations.	22
3.5.4	Nebular phase	24
3.5.5	Spectropolarimetry	24
3.6	Light Curves	26
3.6.1	Understanding Basic Properties of Supernova Light Curves	27
3.6.2	Energy Sources	27
3.6.3	Application to Supernova Types	28
4	Light Curve Analysis	31
4.1	Light curves in different bands from the GIT data	31
4.2	r-band light curve obtained from our pipeline	32
4.3	How does our light curve compare with the light curve from GIT data?	32
4.4	What is the offset between these two light curves?	32
4.5	Conclusions	32

1. Introduction to CCDs and Image Reduction

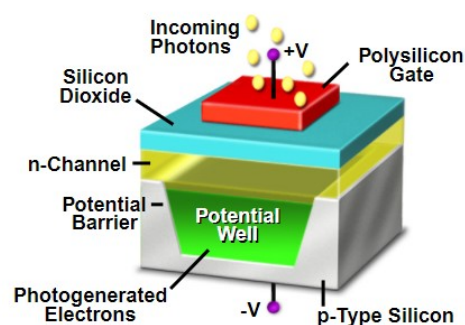
1.1 CCD

Charge Coupled Devices (CCDs) are integral to imaging in astronomy. CCD detectors are widely used for taking images of the sky. These images are processed further to get scientific grade images and are used for astrometry, photometry and spectroscopy. These devices work on the photoelectric effect and employ a clever *readout* technique to get an array of output values which is the representative of the photoelectrons generated due to incoming photons.

1.2 Working

The fundamental light-sensing unit of the CCD is a metal oxide semiconductor (MOS) capacitor operated as a photodiode and storage device. The device consists of an array of these units in the form of 'pixels'.

Silicon (present in the MOS) has a band gap energy of 1.14 electron volts (eV), and so it easily absorbs light of energy 1.1 - 4 eV (11000 to 3000 Å). Photon absorption causes the silicon in the pixels to give up a valence electron and move it into the conduction band. Photons of energy 1.1 eV to near 4 eV generate single electron-hole pairs, whereas those of higher energy produce multiple



pairs (see section 1.3.3) Once electrons have been freed to the conduction band of the silicon, they must be collected and held in place until readout occurs.

Gates are sub-pixel sized electrodes that allow applied voltages to be placed on the pixels. Now, since electrons prefer to occupy positions having lower potential, these applied voltages allow for a potential well (as a consequence of a depletion layer being formed) to collect the freed electrons and hold them till the end of exposure.

This is essential for the readout of the CCD, as the scheme used to readout the collected photoelectrons works by the manipulation of the voltages of these gates.

Cycling through values of certain fixed applied voltages allows the generated charges (the photoelectrons) to be 'coupled' and be shifted along columns of pixels throughout the array.

1.2.1 CCD Readout

Each pixel has 3 gates associated with it each of which can be set to a different potential. Electrons created anywhere within a pixel during the exposure (where each pixel has a surface area equal to the total area under all three gates) will be forced to migrate toward the deepest potential well.

3 Phase Clocking Scheme

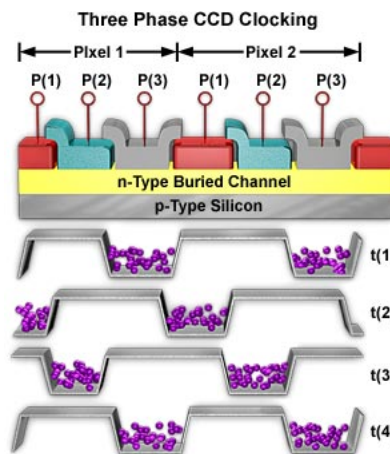


Figure 1

When the exposure is terminated and CCD readout begins, the voltages applied to each gate are cycled (this process is called **clocking the device**) such that the charge stored within each pixel during the integration is electronically shifted. A simple change in the voltage potentials allows the charge to be shifted in a serial fashion along columns from one CCD pixel to another throughout the array.

Each pixel shift occurs for the entire array simultaneously as the columns are connected in parallel.

Each pixel row moves up one column, with the top row being shifted off the array with every clock cycle. The row that is shifted off the array goes into what is called the output shift register or horizontal shift register. Once this happens, and before any further row shifts on the active area occur, each pixel in the output register is shifted out one at a time.

One must remember that none of this shifting of charges is 100% efficient (see section 1.3.4)

Analog-to-Digital

The charge collected within each pixel measured as a voltage and converted into an output digital number through the use of **analog-to-digital converters** [A/D or ADC] (in addition to amplifier circuits to increase signal strength)

- **ADU:**The charge stored in each pixel has an analog value. Each pixel's charge packet is assigned a specific analog-to-digital unit(ADU) or digital number(DN).
- **Gain:**The amount of voltage needed (i.e., the number of collected electrons or received photons) to produce 1 ADU is termed the gain of the device.
- The number of digital bits available in the A/D and the value of the gain that can or should be used for the CCD are connected.(see section

The process of shifting each CCD row into the output register, shifting each pixel along within this register, and performing the voltage conversion of each pixel's stored charge by the A/D to produce a DN value is continued until the entire array of pixels is fully readout.

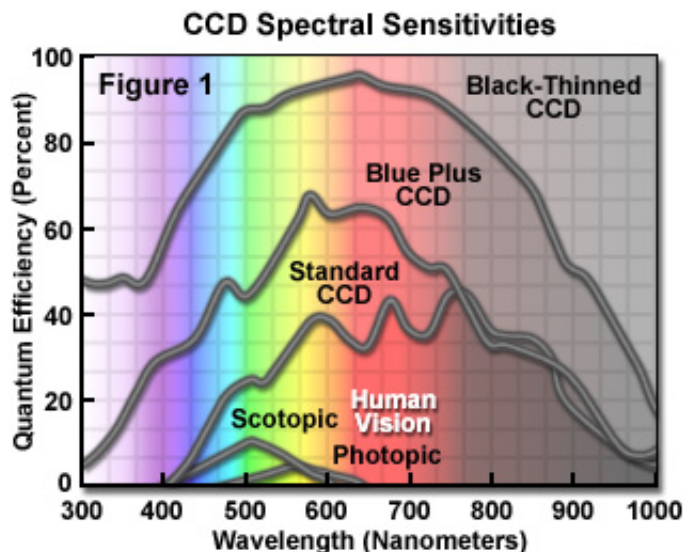
1.2.2 Advantages of CCDs

- Very low noise values (as low as 2-5 electrons)
- Bandwidth from 3000- 11000 Angstroms (in the visible region)
- Shorter readout times
- High Quantum Efficiency (see section 1.3.1)

1.3 Some Useful Terms

1.3.1 Quantum Efficiency

- Quantum Efficiency is defined as the ratio of incoming photons to those actually detected or stored(in the form of photo-electrons) in the device.
- Band-pass: the total wavelength/frequency range for which a detector is sensitive to the incoming photons.
- Quantum efficiency or QE curves allow us to evaluate the relative collecting power of the device as a function of wavelength.



1.3.2 CCD Coatings

- Coating materials allow CCDs to become sensitive to photons normally too blue to allow absorption by the silicon.
- Current processing techniques have reached a state where a given CCD can be “tuned”, via its make-up, resistivity, thickness, and operating temperature, to provide a desired response at a specific wavelength.
- Coating allows the CCD to have increased QE to certain wavelengths.
- Coatings or the use of some form of pre-processor device can also extend the band-pass sensitivity limits.

1.3.3 Gain and Linearity

- **Gain**
 - This determines how the amount of charge collected in each pixel will be assigned to a digital number in the output image.
 - Given in terms of electrons needed to produce 1 ADU step (within the A/D converter)
- An n -bit A/D converter would give output (integral) values in the range of 0 to $2^n - 1$
- CCDs are **linear** in their response over a large range of data values i.e. there is linear relation between the *charge collected within each pixel* and the output value (*digital number stored in the output image*).

Slope of linearity curve gives the gain of the device.

1.3.4 Charge Diffusion and Charge Transfer Efficiency

- **Charge Diffusion:** In some cases, an electron can wander away from its the potential well of its collection pixel and into a neighboring pixel.
- CTE is a measure of the fraction of charge that is successfully transferred to its neighbouring pixel for each cycle of pixel transfer along columns.

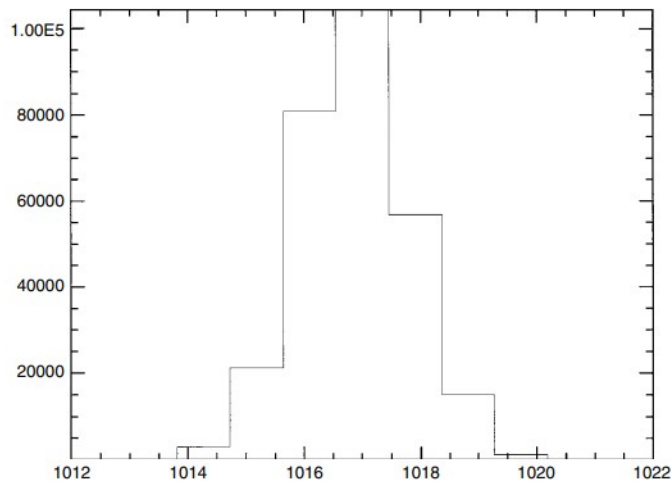
1.3.5 Readout Noise and Dark Current

- **Readout Noise** is quoted in terms of number of electrons introduced per pixel into the final signal upon readout of the device.
 - The conversion from an analog signal to a digital number which is not perfectly repeatable.
 - The electronics may themselves introduce electrons into the entire process, causing unwanted random fluctuations in the output.
- **Dark Current:** Due to inherent thermal noise in the Si lattice, electrons may be freed from the valence band and become collected within the potential well of a pixel. During readout, these dark current electrons become part of the signal.
 - This is why some form of cooling is required for astronomical use.
 - Liquid nitrogen for example is used to cool CCDs used in telescopes to temperatures as low as 0 to -30°C

1.3.6 Bias

- Bias images (taken 'closed shutter') allow one to measure the zero noise level of a CCD. This provides an estimate about the value of an unexposed pixel.

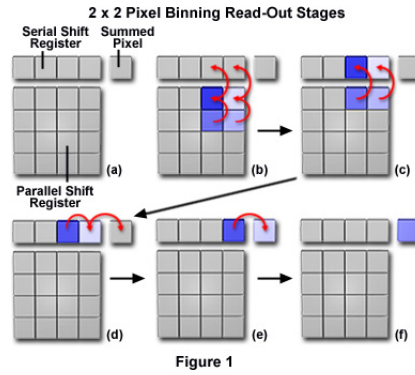
- A 2-D pixel by pixel subtraction of bias image from captured image is required to eliminate underlying noise in the device.
- The histogram of a bias frame having the number of pixels vs. each pixel's ADU value has roughly a Gaussian distribution.
- The width of the distribution σ_{ADU} is related to the read noise of the CCD and the device gain by $\sigma_{ADU} = \frac{\text{Read Noise}}{\text{Gain}}$



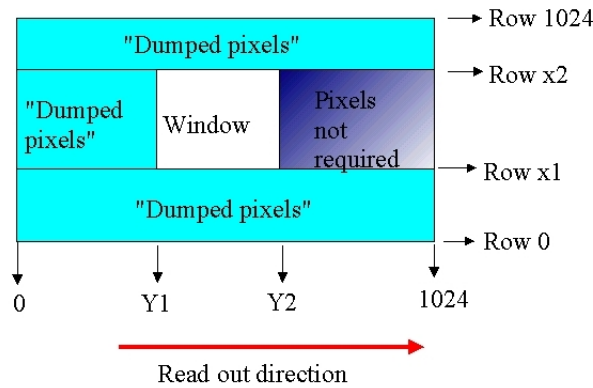
- **Overscan:** They are number of rows or columns used to estimate the electronic bias of the CCD. The CCD may be "overscanned" by adding dummy reads of the electronics without the presence of physical pixels.

1.3.7 Full Well Capacity, Pixel Binning, Windowing

- **Full Well Capacity:** This is the amount of charge a pixel can hold, given in terms of number of electrons.
While this value (high full well capacity) is highly desirable, it is not without compromise. Increasing the full well capacity too much leads to higher charge diffusion.
- **Pixel Binning:** Pixel binning is a clocking scheme used to combine the charge collected by several adjacent CCD pixels (before A/D conversion). The primary benefit of pixel binning is to improve the signal-to-noise ratio in low light conditions at the cost of image resolution. The result of this binning operation will produce only one "superpixel" value, which is digitized and stored in the final image; the original values in each of the four summed pixels are lost forever.



- **Windowing:** Windowing involves choosing a specific rectangular region (or many regions) within the active area of the CCD to be readout.



1.4 Signal-to-Noise Ratio

Signal-to-noise (S/N) ratio compares the level of a desired signal to the level of background noise. A good observational data has a higher value of S/N ratio.

The S/N ratio equation, which is also known as the CCD equation is given as:

$$\frac{S}{N} = \frac{N_*}{\sqrt{N_* + n_{pix}(N_S + N_D + (N_R)^2)}}$$

where, N_* = Number of photons from the object of interest

n_{pix} = Number of pixels under consideration for S/N calculation

N_S = Number of photons from background/sky

N_D = Number of dark current electrons per pixel

N_R = Number of electrons per pixel resulting from Read noise

1.5 Image Data Reduction

Before we can start doing any science with our data, the first step is to clean the image data. We need to remove any noise and imperfections caused in the image. This is done to increase the signal-to-noise ratio.



Following are the different types of images, which we use to clean our observed image data :-

- **Bias Image:** This type of CCD images has an exposure time of zero seconds. We keep the shutter closed and read out the CCD. This image is used to calculate the no signal noise level of the detector. We take as many as 10 bias images, and then take the median of these bias images to get the Master Bias, which is then used for data reduction.
- **Dark Image:** This type of CCD images are taken with shutter closed and an exposure time equals to the exposure time of the object of interest. This image is used to measure the underlying thermal noise and dark current in the CCD. Due to inherent thermal noise in the Si lattice, electrons may be freed from the valence band and become collected within the potential well of a pixel. During readout, these dark current electrons become part of the signal. If provided proper cooling, dark current can be avoided. The common cooling agents used are liquid nitrogen and thermoelectric cooling methods.
- **Flat Fields:** This type of CCD images are obtained by uniform illumination of CCD from dome screens, twilight sky, or quartz lamp projected into a spectrograph. These images are used to correct for pixel-to-pixel variations in the CCD response as well as any non uniform illumination of the detector itself. It also calculates relative Quantum Efficiency of each pixel in the CCD array. We obtain the Master Flat by taking the median of multiple bias subtracted flat field images.

The next step is to get the processed data. This is done using the following equation:

$$\text{Processed Data} = \frac{\text{Raw Data} - \text{Master Bias}}{\text{Master Flat}}$$

1.6 References

-  Cambridge Observing Handbooks for Research Astronomers by Steve B. Howell
-  An Introduction to Astronomical Photometry Using CCDs by W. Romanishin



2. PSF Photometry

In this chapter, the steps in Point Spread Function photometry are discussed with answers to most natural questions one might ask while reading this topic.

2.1 What is PSF?

Stated in oversimplified terms, the Point Spread Function of an imaging system describes the "blurring" of a point source into a spread out blob while imaging it. Ideally one would wish to get a sharp point image for a point object, but this can not happen since any imaging instrument is fundamentally limited. The underlying causes for the specific response of a particular system could be one among a multitude, from instrumental defects to errors introduced by the medium of light's travel, nevertheless, to have a description of these defects as a mathematical function gives important information about how the instrument images any object.

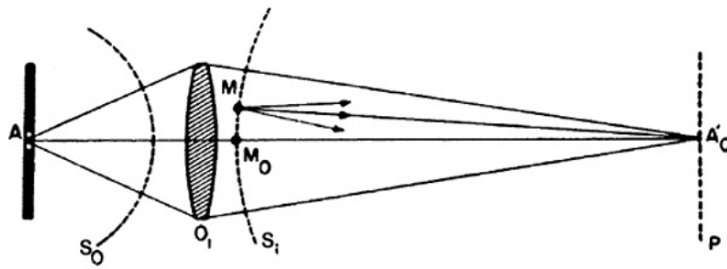
By virtue of being astronomically far from us, we treat luminous objects as point sources (eg. a distant star or a planetary nebula), even though a point source is just a non-physical, mathematical idealisation. If an instrument (say, a telescope) is used to image that object, we get a spread centered around the image point of our intuition. And this is precisely where this almost ubiquitous concept in imaging comes into play.

The PSF is studied widely under Fourier Optics, and is formally defined as the impulse response of a focused optical instrument.

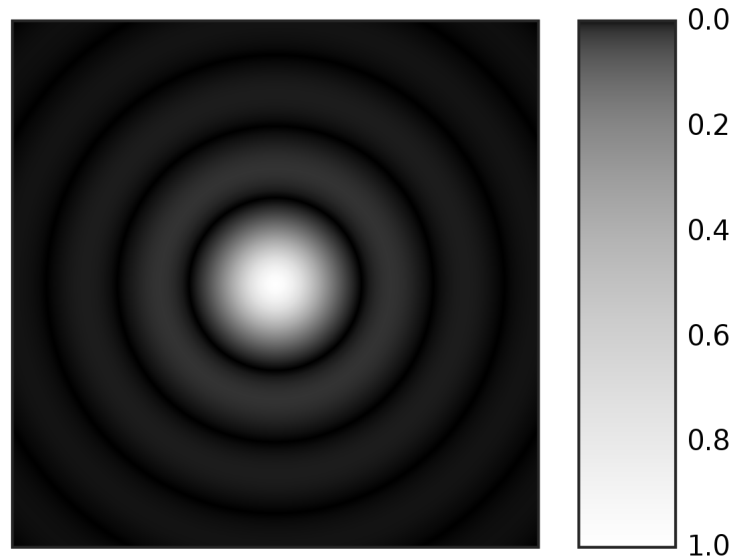
2.2 Why do we get the spread?

When light is emitted from an ideally assumed point object, a fraction of it is collected by the objective and focused at a point in the image plane. Talking a bit too simply in terms of the fundamental phenomena of diffraction and interference, however, we don't get an infinitely small point in the image plane.

Consider an ideal (mathematical non-physical) point source that sends out spherical wavefronts centered at the point. Let us consider a converging lens for the ease of illustration.

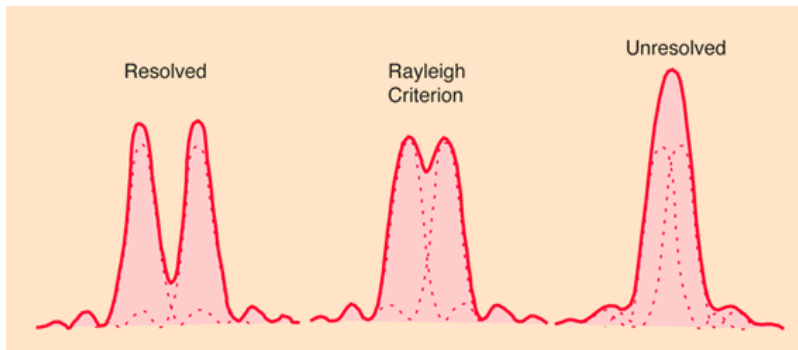


After refraction, we again get another spherical wavefront centered at our intuitive single point image in the image plane. Now, as per Huygen's principle, all points on a wavefront act as individual sources. Thus we get a diffraction pattern or the well-known Airy Disk in the image plane for the point object. The same phenomenon can be understood in the formalism of Fourier Analysis applied to optical systems, which we defer to any textbook on Fourier Optics. We move forth with this basic familiarity with the behaviour of an imaging system, sufficient for the cause of this report.



2.3 Significance of PSF

One may ask why we even care about this non-physical entity. The answer is found yet again in the study of Fourier Optics, where we learn immediately, owing to some convenient mathematical properties of imaging systems, that we can "reverse-engineer" or formally, deconvolve the information about the original source if we know the mathematical function that convolved it. Additionally, since the PSF limits the resolution of the instrument, it can help to understand the Rayleigh criterion of resolution.



We say two objects are just resolved if the first diffraction minimum of the image of one source point coincides with the maximum of another. If the objects are even closer when both the images have a considerable amount of intensity, we get an unresolved hazy picture. Such overlapping configurations of sources can be a common occurrence in astronomical images, and one can see how the study of the instrument's image scrambling behaviour can help in gaining better information about such sources.

2.4 Performing PSF photometry

Working inside Python as our interface, we utilised two other softwares in tandem, that provided all the requisite tools to actually perform PSF photometry, namely Source-extractor (SExtractor) and PSFex. A broad outline of the process involved is given below:

- Source-extractor takes a FITS file as one of the inputs (along with a configuration file and a file instructing which parameters to output) and can automate the entire procedure of photometry, from source detection to photometric estimations and generates an output "catalog" containing the requisite information.
- PSFex then takes the catalog generated by SExtractor as input in FITS_LDAC format to have access to the original image header content.
- PSFex pre-selects detections which are likely to be point sources, based on source characteristics such as half-light radius and ellipticity (flux-radius and elongation in our .param file).
- The PSF modelling process is iterated 4 times. Each iteration consists of computing the PSF model, comparing the vignettes obtained from SExtractor to the model reconstructed in their local contexts, and excluding detections that show too much departure between the data and the model.
- Principal Component Analysis is undergone in each iteration and sinc interpolant is used to fit the model.
- Thus, the final PSF is returned by PSF-ex, mustered by detecting and analysing the sources in that image. The PSF-fit model is itself returned as an image (FITS file)
- This PSF-fit FITS model is fed back to SExtractor, which can now perform PSF photometry to find the fluxes for the sources in the image. The output is again obtained as a catalog.
- We have thus obtained a catalog containing "instrumental" magnitudes detected using SExtractor. To calculate the apparent magnitude, we still require an estimate for the zero point of the image, and to do this, we make use of a queried catalog. We used a catalog containing apparent magnitudes of known, recorded sources queried from Pan-STARRS1. We cross-matched sources that appeared on both catalogs and took the difference to get the zero point.

- To fulfill our goal of obtaining the apparent magnitude of any new, unrecorded source in our image, we can refer back to the SExtractor generated catalog for the instrumental magnitude and correct for ZP to readily obtain our estimate for the apparent magnitude. Here, in this project, the object that we wanted to do this for, was obviously, the supernova SN2018hna.

2.5 How is it beneficial?

A natural question is why to complicate things using PSFEx as we automatically get the job entirely done by SExtractor with mention of apertures.

The answer is yes, aperture photometry is quicker and works very well with a sparsely distributed source field but it fails while tackling a crowded field because some sources may enter into the chosen aperture and ruin the background flux count.

PSF photometry overcomes this by doing away with apertures. It directly makes use of the mathematical elegance of PSF to gain information about the source. If the two sources are at least just resolvable by the instrument, we can use the softwares to readily fit the PSF to the sources, gain flux information and get photometry done.



3. Supernova theory

An understanding of supernova theory is important to understand light curve properly. Supernovae provide us a lot of information such as the physical mechanisms leading to these explosions, the nature of pre and post supernova star, new insights into stellar evolution, insights into nuclear evolution ("chemical evolution"), hubble constant H_0 etc. The following sections briefly present some information regarding search (section 3.1), classification (section 3.2), photometry (section 3.3), and rates (section 3.4) of supernovae. The last two sections (section 3.5, 3.6) present details of spectra and light curves of supernovae.

3.1 Search and Discovery of Supernovae

In the following discussion, redshift (z) is used as a measure of distance (higher redshift corresponding to higher distances). Different equipment and strategies are appropriate for different redshift ranges. Considerations include where to look-the fields and the field of view (FOV); the time interval between successive visits to the fields-the cadence; and the exposure time per visit, which together with telescope aperture determines the limiting magnitude-the depth.

Supernovae in nearby galaxies are bright enough that some are found soon after explosion. Thus nearby events have historically been among the most valuable ones for supernova science. While searching for new supernovae, to obtain a good crop of discoveries, a common practice is to conduct a targeted search of a preselected list of galaxies. But, these targeted searches generally focus on luminous galaxies because within a fixed galaxy type, larger galaxies are expected to produce more supernovae, and observers want to look where supernovae are likely to be found. The price to be paid is a bias in favor of the kinds of supernovae that occur in luminous galaxies.

Relative distances of supernovae in nearby galaxies usually have significant uncertainties because galaxy peculiar velocities, are not negligible compared to the low galaxy recession velocities caused by cosmic expansion. For these galaxies, the use of redshift and the Hubble law does not provide accurate distances. To obtain a sample of supernovae that do have accurate relative distances, optimal for determining absolute-magnitude distributions of the supernova types and other purposes, one wants to reach into the **Hubble flow** (motion of galaxies due solely to the expansion of the Universe).

For high redshift supernovae, deep exposures or the Hubble Space Telescope is used.

3.2 Classification of Supernovae

The primary classification of supernovae is based on the appearance of their optical spectra near maximum light. They are broadly classified into Type I (SN I) and Type II (SN II). Spectra of SN II contain conspicuous hydrogen lines while spectra of SN I do not. Light curves of SN I have predictable regularity, while those of SN II have a variety of shapes. Within these two classes, further classification is also done based on spectral properties and light curve shapes. More information about the spectral properties is provided in section 3.5.

3.3 Photometry

Light curves obtained using photometry can be used to constrain fundamental physical quantities such as the total ejected mass, the mass of synthesized, unstable ^{56}Ni , the kinetic energy of the ejecta, and the radius of the progenitor star. These photometry measurements are usually made in standard broad bands: U, B, V, R, I or u, g, r, i, z in the optical part of the spectrum and often J, H, and K in the near-IR. **Photometric color**, the difference between two broad-band magnitudes, provides coarse information on the spectral energy distribution (SED). More information about light curves is provided in section 3.6.

3.4 Sites, Environments and Rates

After a supernova has been observed, it is sometimes possible to find archival images of the site, which can then be used to detect and characterize the star that exploded.

Spiral and irregular galaxies contain both young and old stars, while elliptical galaxies have only old ones. SN II, SN Ib, and SN Ic are found almost exclusively in spirals and irregulars, and in spirals they tend to occur near the spiral arms, where young stars are concentrated. This is a clear sign that these types are produced by stars that are initially massive (which reached the end of their life before they could drift away from their site of creation). SN Ia are found in all kinds of galaxies and those in spirals show little if any tendency to concentrate to the arms. This indicates that they are produced by stars with smaller initial masses.

Direct detection of more distant progenitors has been successful mainly for SN IIP, yielding more than a dozen confirmed detections of red-supergiant progenitors as well as more than a dozen useful upper limits to the presupernova luminosity. Based on direct detection of progenitors, the inferred ZAMS masses of the progenitors of SN IIP ranged from about 8 to $16M_{\odot}$. The upper value was surprisingly low, because single stars of ZAMS masses up to 25 or $30M_{\odot}$ were expected to produce SN IIP. This anomaly was termed as the “**Red supergiant problem**”. Various explanations for the red-supergiant problem have been proposed. Perhaps stars in the missing mass range collapse directly to produce black holes with little optical display or, for other reasons related to the physics of core collapse, make only weak, dim supernovae that tend not to be discovered.

The environments in which the various supernova types occur also provide statistical information on progenitor masses as well as the ages and metallicities of the stellar populations in which they occur. Like environments, supernova rates in relatively nearby galaxies provide statistical information on progenitors, and a basis for predicting supernova rates in our Galaxy.

3.5 Spectra

Spectroscopic analysis of the light received from the explosion can reveal information about the relative abundances of elements. During the initial days of explosion, a supernova is optically thick and the spectrum forms outside a photosphere. This is called as the **photospheric phase**. As the photosphere recedes deeper layers are revealed for analysis. During the photospheric phase the spectrum consists of a complex series of photon emissions, absorptions, scatterings. Still we will apply certain assumptions such as *local thermodynamic equilibrium* (LTE) as a first-order approximation. Under LTE assumption a matter emits radiation based on the intrinsic properties and temperature. Assumption of LTE for the atomic level populations still holds good when the radiation is decoupled from the electrons. Thus LTE is a decent approximation until appropriate temperature is adopted. For some ions level populations may be nearly in LTE, while for some other ions the level populations strongly depart from being nearly in LTE. A rough rule of thumb is that atoms with lot of transitions, like iron, have excitations closer to LTE while simpler atoms like neutral hydrogen the levels are widely spread.

During the later stages the expanding ejecta becomes optically thin and enters into **nebular phase**. In the nebular phase the conditions are extremely *non-local thermodynamic equilibrium* (NLTE). Because spectral features obtained are usually blended we will compare the observed spectra with synthetic (calculated) spectra, to obtain some deeper interpretation. Obviously there occurs no sharp division between the photospheric phase and nebular phase, but we will model in these two phases to exploit some traditional techniques and approximations.

3.5.1 Elements of line formation in the Photospheric phase

We will try to have an intuitive understanding of the spectral-line formation during the photospheric phase of explosion.

Velocity law.

During the hydrodynamical phase energy is suddenly released inside the star. During this phase of duration, say, t_h the forces on the matter are substantial. After much latter time, the distance a matter travels from the point of explosion is given by $r = vt$ or $v = r/t$, velocity (v) with which the matter travels is directly proportional to the radius (r). This is called as the velocity law. The consequences of velocity law is, the density structure of the ejecta evolves in self similar manner. At a particular radius the density can vary with angle but it scales as t^{-3} during homologous expansion. The velocity gradient is isotropic and homogeneous in nature.

P Cygni line profile.

We first assume spherical symmetry with a sharp photosphere emitting a continuous spectra, photon absorbed by in an atomic transition are immediately emitted in random direction. Let a atomic transition occur at λ_0 . Then the photons scattered towards the observer, from the region closer to the observer are blue shifted ($\lambda < \lambda_0$) while the photons scattered from the farther region are red shifted ($\lambda > \lambda_0$). The region just opposite to the line of sight of the observer are occulted. The photons directed towards the observer suffers more absorption and therefore there is a dip in the flux for blue shifted photons. The photons directed away from the observer are latter scattered towards the direction of line of sight and show emission. So, the combination of both emission and blue shifted absorption is a characteristic of an expanding atmosphere which is called as **P Cygni profile**.

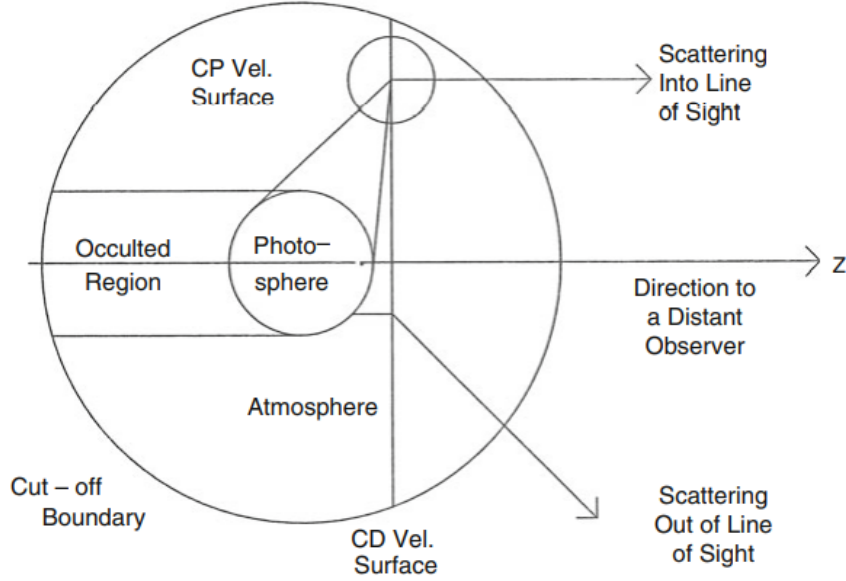


Figure 3.1: Schematic figure of the line-forming layers of a supernova.

Quantitatively, to know a line profile we need to first know the optical depth, $\tau(\nu)$ and the Source function, $S(\nu)$. The **Sobolev approximation** gives an expression for optical depth, $\tau(\nu)$ of the form:

$$\tau(\nu) = \frac{\pi e^2}{m_e c} f \lambda_0 t n_l(\nu) \left[1 - \frac{g_l n_u(\nu)}{g_u n_l(\nu)} \right] \quad (3.1)$$

Where f is the oscillator strength of the atomic transition g_l and g_u are the statistical weight of the lower and upper levels. The term in the square is the correction for stimulated emission.

The source function $S(\nu)$ is given as:

$$S(\nu) = \frac{2hc}{\lambda^3} \left[\frac{g_u n_l(\nu)}{g_l n_u(\nu)} - 1 \right]^{-1} \quad (3.2)$$

For resonant scattering the source function is equal to the mean intensity. Now the wavelength dependence of the intensity beams, I_λ , emitted along the line of sight of the observer is given by using both source function and the optical depth.

$$I_\lambda = S(\nu)(1 - e^{-\tau(\nu)}) \quad (3.3)$$

Where $\tau(\nu)$ and $S(\nu)$ are evaluated at the resonance point. A wave with impact parameter smaller than the radius of the photosphere is

$$I_\lambda = I_{phot} e^{-\tau(\nu)} + S(\nu)(1 - e^{-\tau(\nu)}) \quad (3.4)$$

Where the first term is due to continuum intensity. Finally the flux profile is given by:

$$F_\lambda = 2\pi \int_{p_{min}}^{p_{max}} I_\lambda(p) p dp \quad (3.5)$$

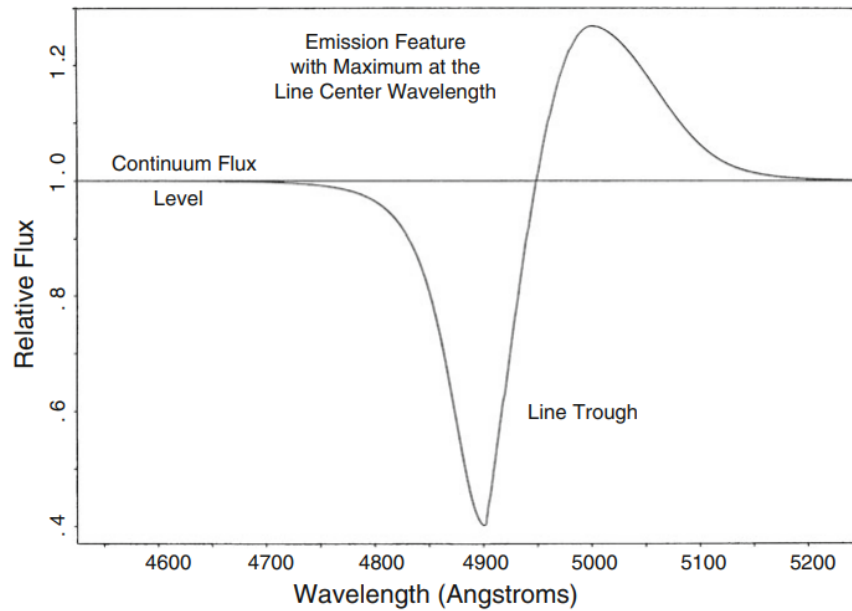


Figure 3.2: P Cygni line profile for a line of rest wavelength 5000\AA and a velocity at the photosphere of $10,000\text{ km/s}$.

Here p is the beam impact parameter in units of photospheric radius.

In the case of sufficiently weak lines, the blue shift of the absorption minimum is due to the velocity of the photosphere. For strong lines the line optical depth is high on common-direction surfaces in front of the photo-disk, the absorption minimum is more likely to be blue shifted. Thus through Sobolev approximation we can see that the density profile of the supernova ejecta need not to be monotonically-declining.

Multiple scattering and Line Blending.

If there is a photon which is scattered by one transition red shifts into resonance with another transition, the photon may be scattered again. This multiple scattering corresponds to the line blending. Due to this reason when making line identifications in photospheric phase of spectra we will concentrate on **absorption minimal**.

3.5.2 Synthetic Spectra for the Photospheric Phase.

SYNOW

The SYNOW supernova-synthetic spectrum code is based on some basic assumptions such as homologous expansion, spherical symmetry, sharp black body photosphere, and resonant-scattering line formation treated in the Sobolev approximation. The code is not suitable for inferring quantitative abundances ratio.

The main function of the code is line identification and determine the velocity at the photosphere, as well as the velocity intervals at which the ions are detected. The optical depth of the reference lines, the velocity at the photosphere and maximum or minimum velocity imposed at the ions, are some important parameters while fitting into an observed spectrum.

For the synthetic spectrum the code requires the atomic partition function and a very large list of

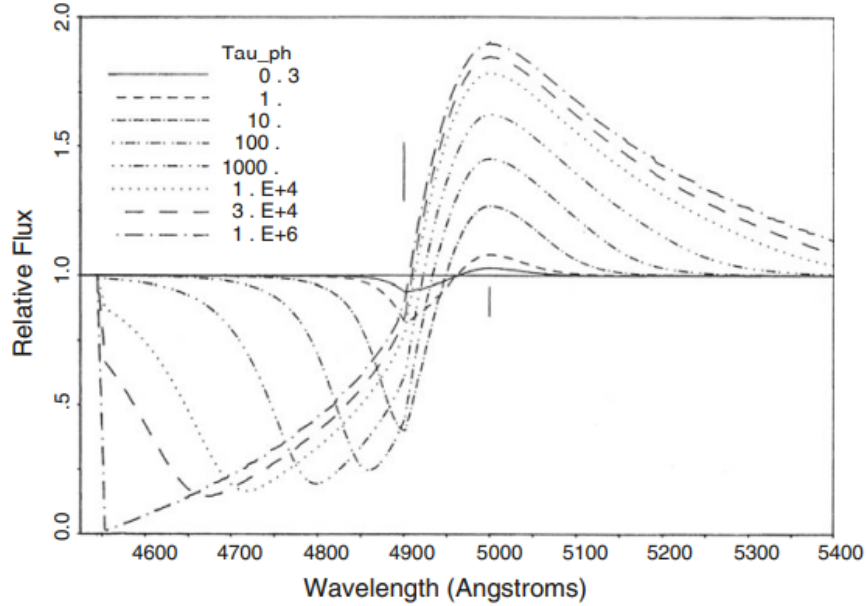


Figure 3.3: Line profiles for $\tau(\nu) \propto \nu^{-7}$ with varying optical depth at the photosphere, Tau_{ph} . The vertical line above the continuum is blue shifted than the vertical line below the continuum. This corresponds to velocity of the photosphere equal to 6000km/s From “Analysis of Supernova Spectra”(Jeffery and Branch)

lines with wavelengths, $\log(gf)$ values and excitation potentials. The SYNOW code is iteration free, therefore the synthetic spectrum can be produced with in seconds. There are certain variations to the main SYNOW code, SYN++ and SYNAPPS, which eases and minimises human interaction.

Monte Carlo

Monte Carlo is a probabilistic method for calculating supernova spectra. Packets of radiant energy are injected into the model ejecta and are tracked through randomized scattering and absorptions. The code assumes Sobolev approximations, sharp blackbody photosphere, and does not solve any rate equation. The difference between SYNOW is input composition and density structures, an approximate radiative-equilibrium temperature distribution, electron scattering in the line forming region. Formal solution for the intensity beams and continuum source functions derived from the packet statistics is taken into account to reduce statistical noise.

3.5.3 Detailed Calculations.

At the expense of computational power more detailed and real physical synthetic spectra can be obtained.

Non-Local Thermodynamic Equilibrium (NLTE).

Even for 1 dimensional case, the ideal calculations should involve, atomic level populations in each radial zones which are obtained by solving coupled NLTE equations, the wavelength dependence mean intensity in each zones, the kinetic temperature in each zone obtained by enforcing energy conservation. In some calculations some or all time dependent terms are neglected so that the

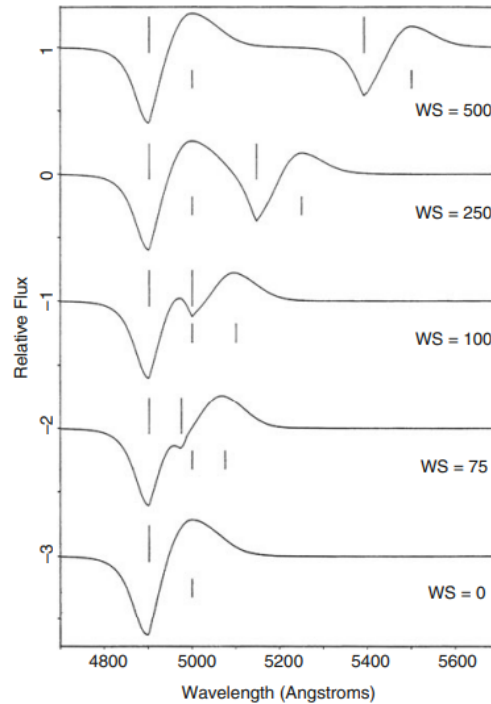


Figure 3.4: Blending of blue line and a weaker red line for various values of wavelength separation.

supernova are modeled in a “snapshot” mode, and the speed of light is taken to be infinite.

Non-thermal Excitation and Ionization.

In supernova we need to take into account the non-thermal ionisation and excitation caused by the products of the nuclear decay. When γ ray undergoes Compton scattering off a free electron a substantial amount of energy is lost. Each original γ ray can lead to numerous excitations and ionizations. Non thermal excitation and ionisation are not important for excitation and ionization that is significantly populated thermally.

Multiple Electron Scattering.

In supernova such as SN II in lines are formed in the regions above the optically thick photosphere where thermalization occurs. In this case the lines formed suffers multiple scattering before emerging to the observer. The details of the line profile depends upon the density and velocity profiles the scattering matter and whether the photons being scattered are internally. Compton scattering could affect the line profile but are usually small in the typical range of temperature and electron velocities. In the Balmer lines these multiple-scattering wings are more prominent. The effect of multiple scattering is also highly prominent for low expansion velocities. For computing line profiles for the photons subjected to multiple scattering we generally use Monte Carlo simulation. We can use several other highly sophisticated codes for synthetic spectra like, PHOENIX, CMFGEN, RAGE/SPECTRUM, HYDRA, powerful Monte Carlo codes such as SEDONA and ARTIS.

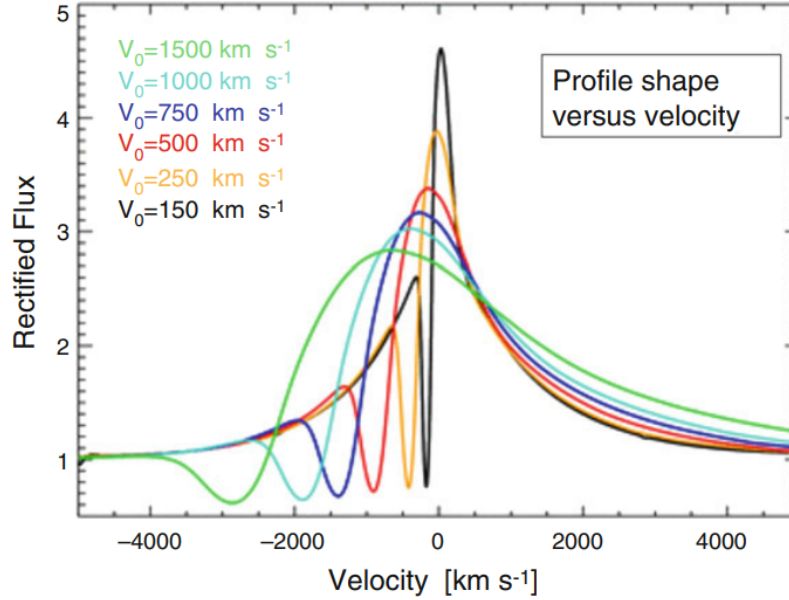


Figure 3.5: Effect of multiple electron scattering on line profiles with decreasing bulk expansion velocity.

3.5.4 Nebular phase

The nebular phase provides direct view into the inner regions of the ejecta, which is powered by radioactive decay primarily that of ^{56}Co . Optical emission lines are produced by recombination, collisional excitation, and fluorescence. Due to expansion in the nebular phase the lines produced tend to be forbidden rather than permitted lines which characterize the higher density photospheric phase. The characteristic line of the nebular phase is the emission peak at the rest wavelength. The nebular phase spectra can provide information of global shape asymmetry and small scale clumping. Modern multi-zone codes for the calculation of nebular-phase synthetic spectra includes NERO. After several years when the atomic processes tend to slow down, we need to take into account the history and time-dependence such as *ionization freezeout*.

3.5.5 Spectropolarimetry

Spectropolarimetry is the study of polarization state of light as a function of wavelength. We know that the supernovae are highly aspherical due to spectropolarimetric data. Polarization of core collapse supernova increases with time which suggests that the asymmetry is stronger in the inner layers. While in the case of Sn Ia the asymmetry is more in the outer layers. Most of the basic understanding regarding the polarized supernovae are based on ellipsoidal model. While real supernovae are undoubtedly more complex, but ellipsoidal model holds good for simpler structures. We can characterise the polarization flux from a source by Stokes parameters (I, Q, U, and V). I is the intensity, Q and U measure the linear polarisation and V measures the circular polarisation. The degree of polarisation is expressed by $P = \sqrt{Q^2 + U^2}/I$ and $\theta = \frac{1}{2}\arctan\frac{U}{Q}$ or,

$$\begin{aligned} Q/I &= P \cos(2\theta) \\ U/I &= P \sin(2\theta) \end{aligned} \quad (3.6)$$

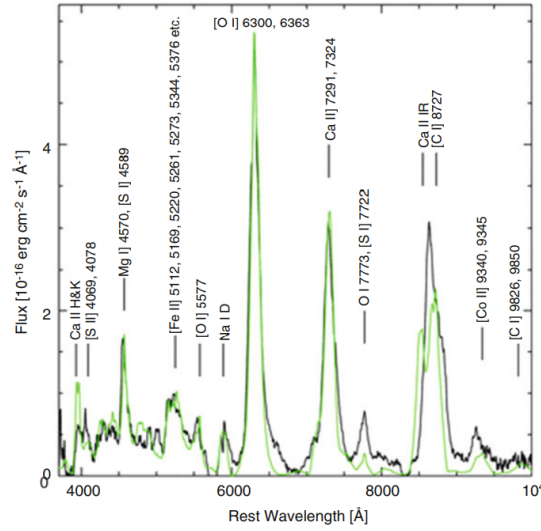


Figure 3.6: Nebular phase spectrum of Type Ic SN 2007gr, obtained 172 days after explosion.

According to astronomical conventions $\theta = 0$ points to the north is the sky.

Errors per pixel are amplified because polarimetry involves the difference between the ordinary and the extraordinary rays. Spectropolarimetry data are plotted in Q/U plane, where the two components correspond to projecting the polarization vectors onto dominant axis and orthogonal axis. The components perpendicular and parallel to the dominant axis are :

$$P_d = ((Q - Q_{ISP})\cos(\alpha) + (U - U_{ISP})\sin(\alpha))/I \quad (3.7)$$

and

$$P_o = -((Q - Q_{ISP})\sin(\alpha) + (U - U_{ISP})\cos(\alpha))/I \quad (3.8)$$

Here Q_{ISP} and U_{ISP} are the Stokes parameters of the ISP. The spectral profile are not sensitive to the choice of ISP.

The spectropolarimetric types are: **SP Type N0**: In this case the data are consistent with the observational errors and there is no measurable supernova polarization.

SP Type N1: In this the data does not show elongation in any particular direction. The data indicates intrinsic polarization or underestimation of errors.

SP Type D0: In this case the data forms an elongated ellipse. The locus of the data can be approximated by straight line.

SP Type D1: In this the data forms an elongated ellipse with the deviation along the orthogonal axis being significant.

SP Type L: In this the data shows loops in the Q/U plane due to large changes in amplitude and position angle across spectral lines.

The SP type may evolve because the supernova undoubtedly evolves in wavelength and time. Thus, we can say that the spectropolarimetric tools provide an opportunity to explore the supernovae asymmetry.

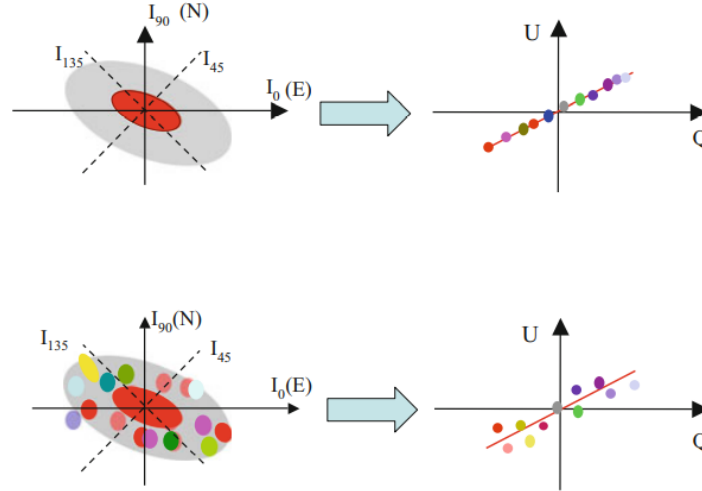


Figure 3.7: **Top left:** A smooth, axis symmetric structure. Direction denoted by I represent the measurement of flux at angles needed to construct the Q/U polarization components. **Top right:** The resulting wavelength-dependent polarization amplitude plotted in the Q/U plane follows a straight line. The colored circles represent the polarization measured at different wavelengths. **Lower left:** Case where the matter is distributed in clumps. **Lower right:** The polarization distribution in the Q/U plane does not follows a straight line.

3.6 Light Curves

Light curves display the temporal evolution of the energy released by a cosmic object. Light curves provide an important source of information about the physics of objects that change their brightness over time, such as novae, supernovae, and variable stars. This record of the variability of brightness helps astronomers understand the processes at work and helps them determine specific events in the stellar evolution. Light curves of Supernovae are categorized into multiple types giving key insights into their sources of energy and their evolution.

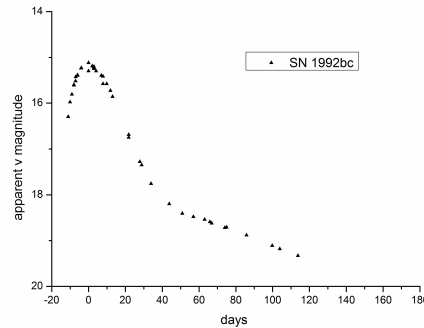


Figure 3.8: SN1992bc Light Curve

3.6.1 Understanding Basic Properties of Supernova Light Curves

Several weeks after the explosion, the supernova reaches its maximum brightness at a radius of $\sim 10^{15}$ cm. At this point, the photospheric temperature is $\sim 10^4$ K, and the velocity of the photosphere is $\sim 10^4$ km s $^{-1}$. These are the characteristic values of our supernova. The star's core is the region that powers the explosion. It is comparable to the radius of Earth, $R_c \sim 10^8$ cm. The outer regions of the stars are lightly bounded and hence are easy to expel. A true explosion must disrupt the core. In other words, it should overcome its binding energy. For the given R_c the binding energy of the core is

$$\frac{GM^2}{R_c} \sim 10^{51} \text{ erg or } 1B$$

This is the basic energy scale for most supernova explosions. The energy per unit masses is associated with the explosion velocity, which is essentially its escape velocity from the core

$$v \sim \sqrt{\frac{2GM}{R_c}} \sim 10^4 \text{ km s}^{-1}$$

The fundamental properties of the light curve depend on two timescales: the time for photons to diffuse out, and the time for the supernova to expand. Radiation diffuses out via the photon random walk. The photon mean free path is $l \sim 1/\kappa\rho$, where ρ is the density, so the photon requires about $N \sim (R/l)^2$ steps to travel distance R . Given that the time flight for each step is l/c , the diffusion time is

$$t_{diff} \sim \frac{Nl}{c} \sim \frac{R^2}{lc} \sim \frac{\tau R}{c}$$

Here, τ is the optical depth.

Maximum luminosity occurs when the diffusion time is comparable to the dynamic time. This occurs when $\tau \simeq 30$. Its important to note that maximum light is not when the ejecta turns transparent, as one might naturally expect, and that the optical depth at maximum light is roughly independent of the opacity.

3.6.2 Energy Sources

Various energy sources and radiation mechanisms shape the light curves of supernovae.

Shock Energy: Breakout, Fireball, and Plateau

When a star goes supernova, a shock wave is generated that approaches the surface of the star. The shock and the post-shock regions are radiation-dominated. As the optical depth between the shock and the photosphere of the progenitor star becomes low enough, the supernova starts to brighten as that radiation can finally begin to escape. This escape of radiation is known as breakout that typically occurs when the shock is at an optical depth of $\tau \simeq \frac{c}{v} \simeq 30$. For asymmetric explosions, the shock reaches the surface at different times. The breakout leads to a release of energy. The total energy radiated is $E_{bo} \simeq 8\pi R_o^2 \kappa^{-1} c v_{bo}$. Here, v_{bo} is the shock velocity at breakout.

For core-collapse supernovae and SN Ia, the radiated energies are $\gtrsim 10^{46}$ and $\lesssim 10^{42}$ ergs, respectively. Post breakout, the hot, shocked ejecta is exposed. Adiabatic expansion of the ejecta cools the system, which causes the luminosity to decline. There occurs what we call as fireball phase in which the UVOIR luminosity decreases monotonically. As discussed above, when a progenitor of a smaller radius explodes, adiabatic expansion severely reduces the temperature before the condition $\tau \simeq c/v$ is attained and any fireball phase is brief. This applies to SN Ia, SN Ib, and SN Ic.

Radioactive Decay of ^{56}Ni and ^{56}Co

During the explosion, a material with equal numbers of protons, Z , and neutrons, N , is burned rapidly (~ 1 s), allowing little time for electron captures or beta decays to change the Z/N ratio. At the nuclear-statistical equilibrium, ^{56}Ni happens to be the most tightly bound nucleus with $Z = N$. An unstable ^{56}Ni captures an electron and decays into ^{56}Co with a half-life of 6.1 days. In turn, ^{56}Co decays to stable ^{56}Fe , 81% of the time by electron capture and 19% by positron decay. Following is the full reaction:-

Electron capture of ^{56}Ni : $^{56}\text{Ni} + e^- \rightarrow ^{56}\text{Co} + \nu_e + \gamma$

Decay time: $\tau_{\text{Ni}} = 6.1\text{d}$

Energies of the most important γ 's: 750keV, 812keV, 158keV

Electron capture of ^{56}Co (81%) : $^{56}\text{Co} + e^- \rightarrow ^{56}\text{Fe} + \nu_e + \gamma$

β -decay of ^{56}Co (19%) : $^{56}\text{Co} \rightarrow ^{56}\text{Fe} + e^+ + \gamma + \nu_e$

Decay time: $\tau_{\text{Co}} = 77.1\text{d}$

Energies of e^+ 's: about 600keV (Energies of the most important γ 's: 847KeV, 1.238 MeV)

It's a cosmic coincidence that the decay times of ^{56}Ni and ^{56}Co are roughly the same as the timescale on which a solar mass of material exploded with 1 B of energy becomes nearly optically thin. This allows SN Ia to shine brightly.

Gamma-Ray Light Curves

The hard photons from the radioactive decay that manage to escape the ejecta cause heating and subsequently power the UVOIR light curve.

Buried Pulsar/Magnetar

Pulsar discovery lead to the inspection of effects due to formation of a compact object on the energetics and luminosity of a supernovas. To provide the energy of a supernova explosion, the magnetic field must be very high, 10^{14} G, in the range of magnetars, but more modest fields could still produce appreciable luminosity. The expression for the light curve of a supernova powered by a pulsar or magnetar is:-

$$L(t) = \frac{E_p}{t_p} e^{-x^2/2} \int_0^x e^{z^2/2} \frac{z}{1+yz} dz$$

Here,

t_p the characteristic timescale for spin-down.

E_p initial rotational energy of the pulsar

t_{eff} the effective diffusion time

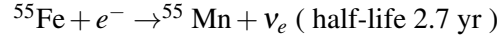
$x = t/t_{eff}$ and $y = t_{eff}/t_p$

3.6.3 Application to Supernova Types

SN Ia

Radioactive decay is the main source of energy that powers the light of the curve of SN Ia. A typical SN Ia reaches its maximum luminosity $L_{UVOIR} \gtrsim 10^{43} \text{erg s}^{-1}$ in about 20 days after the explosion. After about 200 days, all the gamma rays escape and the light curve is dependent on positrons. In the limit of a sufficiently strong and tangled magnetic field, positrons are trapped and deposit their kinetic energy by collisions with electrons before slowing down and annihilating with electrons to produce 0.511MeV -rays, which escape. While the energy deposition is dominated by trapped

positrons, the slope of the bolometric light curve should match the ^{56}Co decay rate. ^{55}Fe may also contribute a significant amount of energy to our light curve.



SN Ia produce large quantities of iron-group isotopes, the decay of ^{55}Fe is likely to be more important for them.

SN Ib/c

The SN Ib/c light curves are formed due to the core-collapse of massive star progenitors that have lost their hydrogen envelopes have radii in the range $0.1\text{--}1 R_\odot$. They are observed to be highly polarized, due to asymmetries. Just like SN Ia, post fireball phase the light curve is powered by the radioactive decay of ^{56}Ni and ^{56}Co . Fundamentally both have a similar physical process but differ by ejected mass, kinetic energy, compositions, opacities, and asymmetries.

SN Iib

Unlike SN Ib/c, the progenitor star of SN Iib has not lost all of its hydrogen envelopes by means of a stellar wind. Due to this the progenitor star has a larger radius allowing for a longer period of fireball phase.

SN IIP

With a massive hydrogen envelope of about $10M_\odot$, the progenitor star has a light curve plateau in SN IIP. The shock wave takes hours and days to reach the photosphere. Breakout has not yet been observed for an SN IIP. The duration of the plateau, typically ~ 100 days, is determined by the mass of the hydrogen envelope, the kinetic energy, and the extent to which ^{56}Ni is mixed towards the surface.

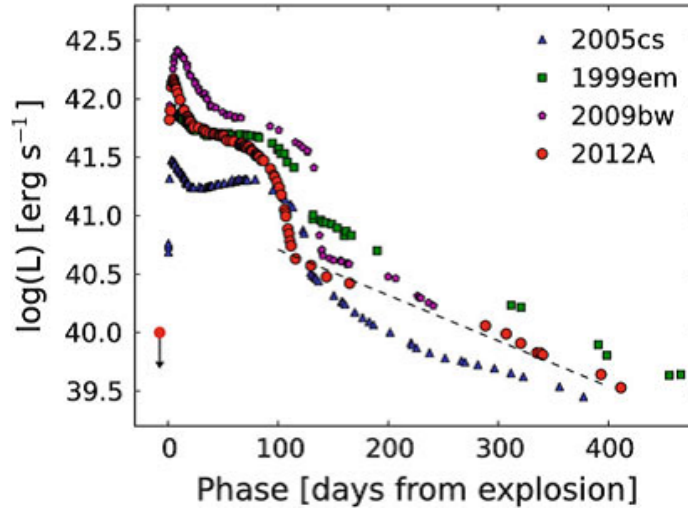


Figure 3.9: UVOIR light curves of four SN IIP. The dashed line shows the ^{56}Co decay rate

4. Light Curve Analysis

4.1 Light curves in different bands from the GIT data

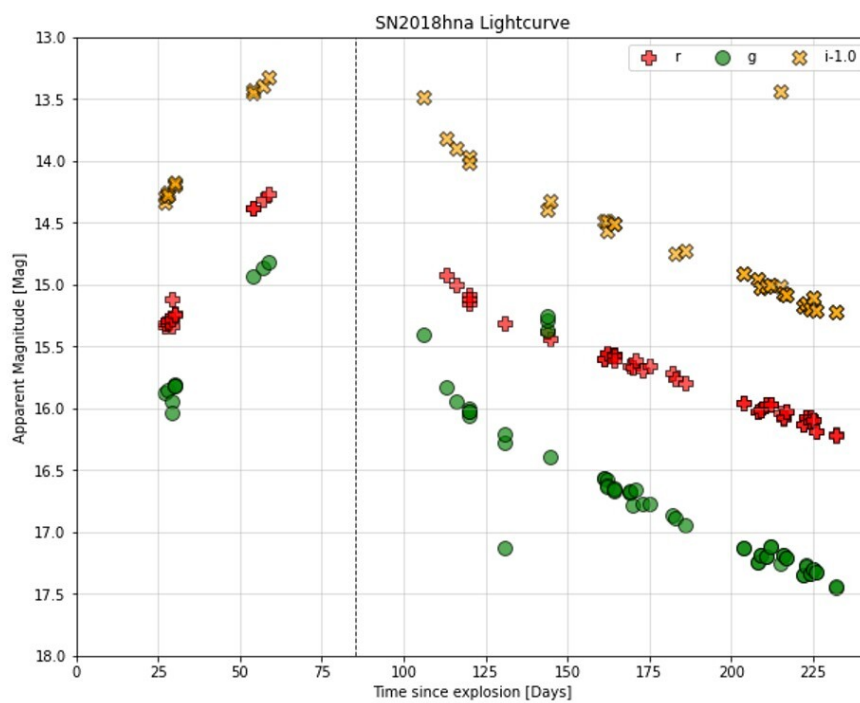


Figure 4.1: Lightcurve obtained from GIT data

These are the light curves we will be using as a reference to compare the results that we obtained from feeding GIT images in our pipeline.

4.2 r-band light curve obtained from our pipeline

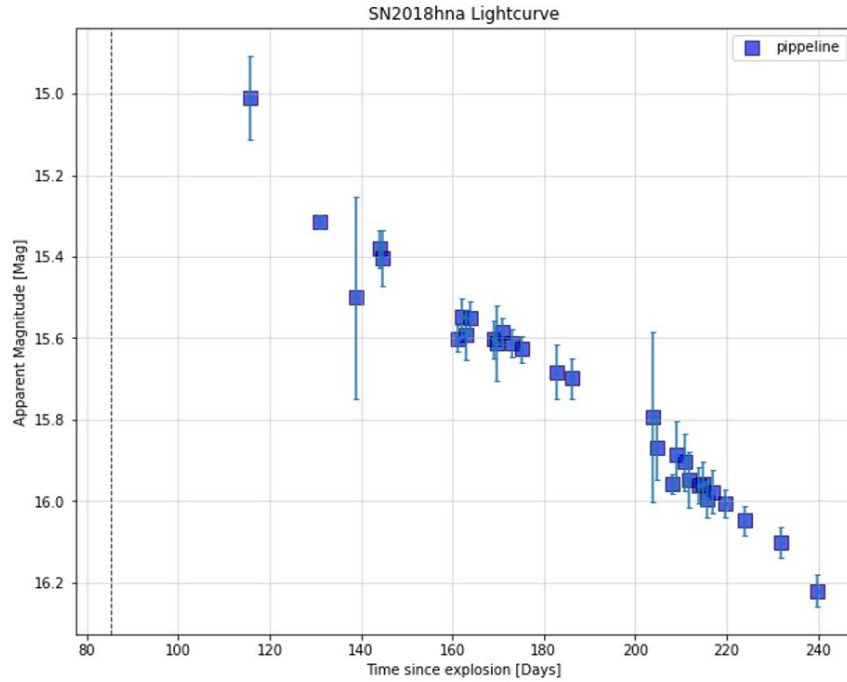


Figure 4.2: Lightcurve from pipeline

We fed SN2018hna images obtained at different times in the r-band obtained from GIT into our pipeline. The pipeline automatically performed PSF photometry on each image, obtained the magnitudes and errors, and then plotted the light curve. The above image is the result obtained from our pipeline.

4.3 How does our light curve compare with the light curve from GIT data?

Plotting the r-band light curves from the GIT data and from our pipeline in the same graph, we can see that our pipeline did pretty well.

4.4 What is the offset between these two light curves?

We found the all the common time points between the two data sets, and plotted them (second figure of the plot). We then calculated the difference between the magnitudes at those common-time points. The first figure of the plot shows that this offset (i.e., magnitudes from pipeline data subtracted from the corresponding magnitudes from the GIT data) is positive at each point. Also, the offset doesn't cross 0.175 mark.

4.5 Conclusions

- The Supernova magnitude rises with time, reaches a maximum and then declines in all bands.

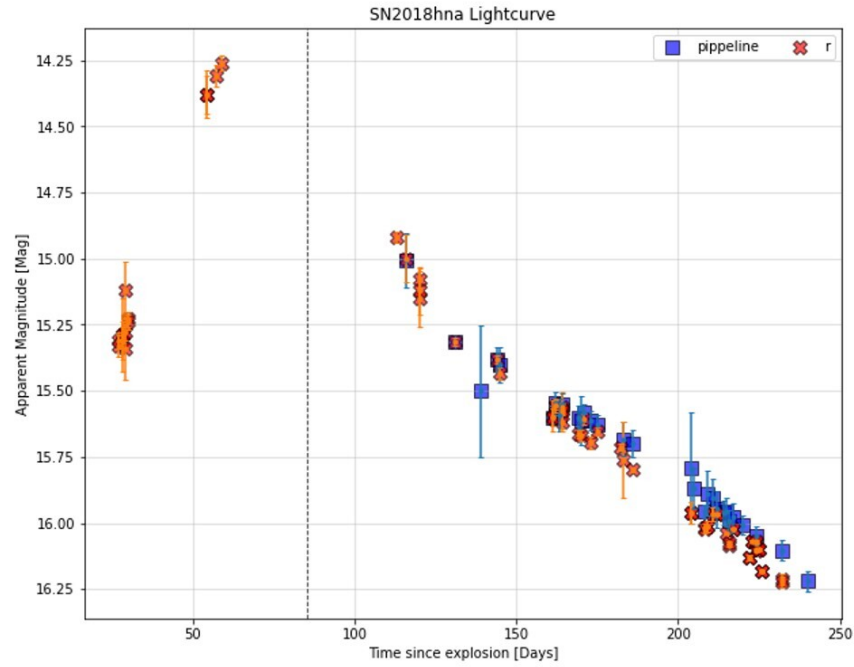


Figure 4.3: Comparison between GIT data and pipeline results

- Initial the photons struggle to escape the ejecta as the SN is optically thick.
- At maximum magnitude, time scale of diffusion of photons \approx time scale of expansion of ejecta. Fundamental properties of light curve depend on these two time scales.
- Broadness of a Light curve directly related to the amount of mass in the ejecta. Broader the light curve, more matter in the ejecta. Light curve in each band is constructed via the contribution of different elements produced in the SN explosion. Therefore, light curve can help understand the amount matter of a particular element
- High energy photons from the SN explosion are reprocessed in the ejecta to optical photons. This mechanism enables us to view them in optical bands.

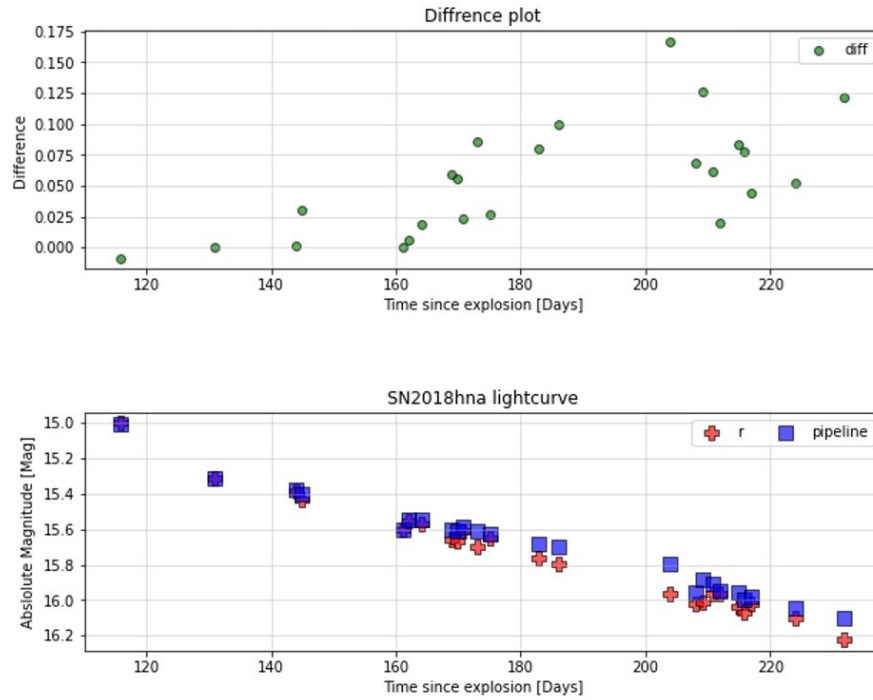


Figure 4.4: Offset between pipeline results and GIT data

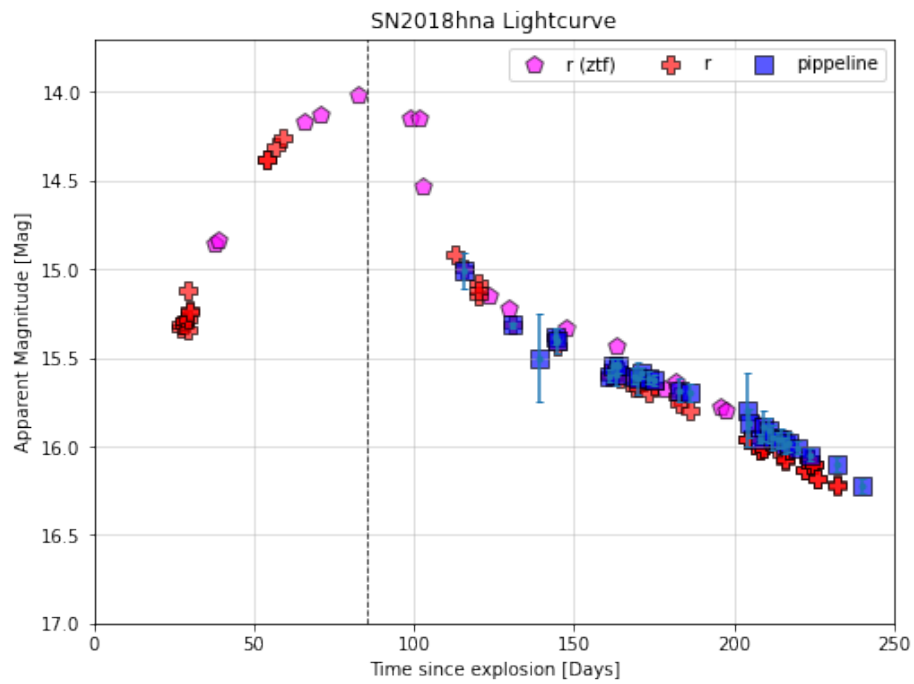


Figure 4.5: r band lightcurve with ZTF data